A new algorithm for extended nonequilibrium molecular dynamics simulations of mixed flow

Thomas A. Hunt, Stefano Bernardi, and B. D. Todd

Citation: The Journal of Chemical Physics **133**, 154116 (2010); doi: 10.1063/1.3489683
View online: http://dx.doi.org/10.1063/1.3489683
View Table of Contents: http://scitation.aip.org/content/aip/journal/jcp/133/15?ver=pdfcov
Published by the AIP Publishing

A new algorithm for extended nonequilibrium molecular dynamics simulations of mixed flow

Thomas A. Hunt,[1,a)] Stefano Bernardi,[2,b)] and B. D. Todd[2,c)]
[1]*Computational Biophysics, University of Twente, P.O; Box 217, 7500 AE Enschede, The Netherlands*
[2]*Centre for Molecular Simulation, Swinburne University of Technology, Hawthorn, Victoria 3122, Australia*

(Received 23 June 2010; accepted 25 August 2010; published online 21 October 2010)

In this work, we develop a new algorithm for nonequilibrium molecular dynamics of fluids under planar mixed flow, a linear combination of planar elongational flow and planar Couette flow. To date, the only way of simulating mixed flow using nonequilibrium molecular dynamics techniques was to impose onto the simulation box irreversible transformations. This would bring the simulation to an end as soon as the minimum lattice space requirements were violated. In practical terms, this meant repeating the short simulations to improve statistics and extending the box dimensions to increase the total simulation time. Our method, similar to what has already been done for pure elongational flow, allows a cuboid box to deform in time following the streamlines of the mixed flow and, after a period of time determined by the elongational field, to be mapped back and recover its initial shape. No discontinuity in physical properties is present during the mapping and the simulation can, in this way, be extended indefinitely. We also show that the most general form of mixed flow, in which the angle between the expanding (or contracting) direction and the velocity gradient axis varies, can be cast in a so-called canonical form, in which the angle assumes values that are multiples of π (when a mixed flow exists), by an appropriate choice of the field parameters. © *2010 American Institute of Physics*. [doi:10.1063/1.3489683]

I. INTRODUCTION

Homogeneous nonequilibrium molecular dynamics (NEMD) techniques have been successfully employed to characterize the rheology of many classes of simple and polymeric fluids because they allow one to study bulk properties by means of synthetic algorithms combined with appropriate periodic boundary conditions (PBCs). PBCs have to be compatible with each particular type of flow one wants to simulate, so as not to introduce any spurious dynamics. Finding PBCs for every type of flow is still an open problem. Standard flows can be divided into shear and shear-free flows according to the value of the off-diagonal components of the strain-rate tensor (shear-free flow corresponds to the case of zero off-diagonal components). We will concentrate our attention on planar flows. Many studies have been done on planar shear flow [planar Couette flow (PCF)] and fewer on planar elongational flow (PEF); because they are simple to characterize, efficient simulation techniques have already been implemented and they are present in almost every real flow situation. Even if these flows are simplifications, their study has proven to be useful in understanding many industrial processes such as extrusion, injection molding, and sheet casting, but also in biological systems such as DNA chain dynamics.[1] For simple PCF, the Lees–Edwards PBCs (Ref. 2) make it possible to extend a simulation for an arbitrary amount of time. Unfortunately, these are *ad hoc* PBCs and it is not possible to generalize them to other flow geometries. A general PBC procedure, applicable to every flow, requires the deformation of the simulation box to follow the streamlines of the flow. However, the simulation can be extended indefinitely only if it is possible to perform a mapping of the cell such that the initial configuration is periodically recovered (without causing any discontinuity in the physical properties). For the remapping to take place, two conditions have to be met simultaneously: the underlying lattice, from which the cell box is generated, has to be both compatible and reproducible. Compatibility means that there is a finite minimum spacing between lattice points; reproducibility means that the lattice can, at two different times, be generated by two equivalent basis vectors, i.e., the lattice points at two different times occupy the same positions in space.[3] This has been shown for PCF (Lagrangian-rhomboid PBCs), for which the conditions for the remapping optimization have been derived,[4] and for PEF by Kraynik and Reinelt,[5] but for other geometries it can be difficult, if not impossible. An extensive description of lattice properties can be found in Refs. 3 and 6.

Kraynik and Reinelt[5] provided, for the first time, the conditions necessary for both reproducibility and compatibility of arbitrary lattices for planar extensional flow with respect to multiphase flows. Their results were used by Todd and Daivis[7] and Baranyai and Cummings[8] to independently realize NEMD PBCs for planar extensional flow. More recently, Hunt and Todd[9] showed that the Kraynik–Reinelt

[a)]Electronic mail: t.a.hunt@tnw.utwente.nl.
[b)]Electronic mail: sbernardi@ict.swin.edu.au.
[c)]Electronic mail: btodd@swin.edu.au.

PBCs are related to the Arnold cat map and derived much simpler mathematical rules to find the necessary conditions for the remapping. Furthermore, Matin *et al.*[10] provided a new cell list algorithm to reduce the computation time for large systems.

In this work, we show how to derive compatible and reproducible PBCs for planar mixed flow (PMF), a linear combination of planar shear and planar elongation, characterized by nonzero values of both diagonal and off-diagonal components of the strain-rate tensor. As stated above, fluids in real situations can simultaneously show a combination of several types of flows, hence the importance of developing techniques that extend the range of flows that can be characterized. Up until now, simulations of fluids undergoing mixed flow were performed through an irreversible deformation of the cell box,[11] bringing the simulation to an end when the minimum distance requirements were broken. This clearly restricted the available length of the simulations, and the complexity of the systems which could be studied.

Brownian dynamics techniques alternatively can be used for the characterization and study of single molecular chains in solution[1,12,13] undergoing any kind of flow; however, because of the impossibility of simulating interactions among multiple units, they are not suitable for dense fluids. For planar elongation, two alternative ways to overcome time limits have been attempted: by means of the transient time correlation function technique[14] and by using frequency dependent strain-rate techniques.[15,16] The first approach allows one to improve statistics for NEMD algorithms with a limited simulation time, while the latter allows the extrapolation of properties of interest at the zero frequency limit. Neither method has been employed for mixed flow to our knowledge. However, recently a hybrid MD-MC coarse-grained method that does not rely on the implementation of periodic boundary conditions has been devised and tested for short chain systems for various flow geometries in the weak field limit.[17] Like all such schemes, it is unsuitable in the strongly nonlinear regime.

The idea for indefinitely extended PBCs for mixed flows relies on the possibility of finding reproducible lattices for any homogeneous and isochoric flow with a diagonalizable velocity gradient tensor.[5] The application of this idea to NEMD simulations of mixed flow has already been outlined in the Ph.D. thesis of Hunt.[18]

II. THEORY

The algorithm we present in this section makes use of the results concerning both lattice reproducibility and compatibility, some of which are outlined by Kraynik and Reinelt.[5]

A general lattice can be written at time $t=0$ as a set of points

$$\mathbf{L}_i(0) = n_1\mathbf{l}_1(0) + n_2\mathbf{l}_2(0) + n_3\mathbf{l}_3(0), \tag{1}$$

where n_k is a set of integers and $\mathbf{l}_i(0)$ are linearly independent lattice vectors. The time evolution for the lattice is given by

$$\mathbf{L}_i(t) = \mathbf{L}_i(0)\cdot\mathbf{\Lambda}, \tag{2}$$

where $\mathbf{\Lambda}=\exp(\boldsymbol{\nabla}\mathsf{u}t)$ and $\det\mathbf{\Lambda}=1$. For PEF, the velocity gradient $\boldsymbol{\nabla}\mathsf{u}$ is constant, traceless, and diagonal.

The lattice is reproducible only if for some integers N_{ij}

$$\mathbf{L}_i(t=\tau_p) = \mathbf{L}_i(0)\cdot\mathbf{\Lambda} = N_{i1}\mathbf{l}_1(0) + N_{i2}\mathbf{l}_2(0) + N_{i3}\mathbf{l}_3(0) = \mathbf{L}_i(0), \tag{3}$$

where τ_p is the reproducibility time. However, Kraynik and Reinelt[5] noted that $\boldsymbol{\nabla}\mathsf{u}$ can be replaced by any diagonalizable constant matrix with real eigenvalues and zero trace. In fact, if $\boldsymbol{\nabla}\mathsf{u}=\mathsf{S}\cdot\mathsf{D}\cdot\mathsf{S}^{-1}$ with D a diagonal matrix, a new set of basis vectors

$$\mathbf{l}_i'(0) = \mathbf{l}_i(0)\cdot\mathsf{S}^{-1} \tag{4}$$

exists, which is reproducible under the flow generated by $\boldsymbol{\nabla}\mathsf{u}$. The tensor S^{-1} represents, therefore, a mapping necessary to make the old basis $\mathbf{l}_i(0)$ reproducible in the new flow geometry. If a diagonalization can be performed

$$\mathbf{\Lambda} = \exp(\boldsymbol{\nabla}\mathsf{u}t) = \exp(\mathsf{S}\cdot\mathsf{D}\cdot\mathsf{S}^{-1}t) = \mathsf{S}\cdot\exp(\mathsf{D}t)\cdot\mathsf{S}^{-1}, \tag{5}$$

it follows that

$$\begin{aligned}\mathbf{L}_i'(t=\tau_p) &= \mathbf{L}_i'(0)\cdot\mathbf{\Lambda} = \mathbf{L}_i(0)\cdot\mathsf{S}^{-1}\cdot\mathsf{S}\cdot\exp(\mathsf{D}t)\cdot\mathsf{S}^{-1}\\ &= \mathbf{L}_i(0)\cdot\exp(\mathsf{D}t)\cdot\mathsf{S}^{-1} = N_{i1}\mathbf{l}_1(0)\cdot\mathsf{S}^{-1}\\ &\quad + N_{i2}\mathbf{l}_2(0)\cdot\mathsf{S}^{-1} + N_{i3}\mathbf{l}_3(0)\cdot\mathsf{S}^{-1}\\ &= N_{i1}\mathbf{l}_1'(0) + N_{i2}\mathbf{l}_2'(0) + N_{i3}\mathbf{l}_3'(0).\end{aligned} \tag{6}$$

This expression is equivalent to Eq. (3), but in the new basis $\mathbf{l}_i'(0)$.

For the development and testing of our algorithm, we consider a velocity gradient tensor of the form

$$\boldsymbol{\nabla}\mathsf{u}^c = \begin{pmatrix}\dot\epsilon & 0 & 0\\ \dot\gamma & -\dot\epsilon & 0\\ 0 & 0 & 0\end{pmatrix} \tag{7}$$

that we call "canonical" and in which the expanding/contracting directions are, respectively, along the x and y axes, with elongational field strength $\dot\epsilon$ and shear gradient $\dot\gamma$ along the y direction. We note that other parameterizations for the velocity gradient are possible (see, for example, Refs. 19 and 20). The canonical velocity gradient tensor can be diagonalized as follows:

$$\begin{aligned}\boldsymbol{\nabla}\mathsf{u}^c &= \begin{pmatrix}\dot\epsilon & 0 & 0\\ \dot\gamma & -\dot\epsilon & 0\\ 0 & 0 & 0\end{pmatrix} = \begin{pmatrix}1 & 0 & 0\\ \frac{\dot\gamma}{2\dot\epsilon} & 1 & 0\\ 0 & 0 & 1\end{pmatrix}\begin{pmatrix}\dot\epsilon & 0 & 0\\ 0 & -\dot\epsilon & 0\\ 0 & 0 & 0\end{pmatrix}\\ &\quad\times\begin{pmatrix}1 & 0 & 0\\ -\frac{\dot\gamma}{2\dot\epsilon} & 1 & 0\\ 0 & 0 & 1\end{pmatrix} = \mathsf{S}\cdot\mathsf{D}\cdot\mathsf{S}^{-1}.\end{aligned} \tag{8}$$

The diagonal matrix D is the velocity gradient for PEF, for which Kraynik and Reinelt[5] had already identified a set

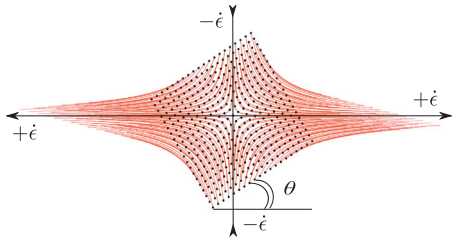

FIG. 1. Initial configuration for a lattice (black dots) undergoing planar elongational flow and corresponding streamlines (red lines). The contracting and expanding axes are orthogonal.

of orthogonal, reproducible, and compatible basis vectors $\mathbf{l}_i(0)$. We can therefore apply the mapping of Eq. (4) and obtain a reproducible lattice under mixed flow

$$\mathbf{l}_1'(0) = \mathbf{l}_1(0)\cdot \mathsf{S}^{-1} = (\cos\theta, \sin\theta, 0)\cdot \mathsf{S}^{-1} = \left(\cos\theta - \frac{\dot{\gamma}}{2\dot{\epsilon}}\sin\theta, \sin\theta, 0\right),$$

$$\mathbf{l}_2'(0) = \mathbf{l}_2(0)\cdot \mathsf{S}^{-1} = (-\sin\theta, \cos\theta, 0)\cdot \mathsf{S}^{-1} = \left(-\sin\theta - \frac{\dot{\gamma}}{2\dot{\epsilon}}\cos\theta, \cos\theta, 0\right), \tag{9}$$

$$\mathbf{l}_3'(0) = \mathbf{l}_3(0)\cdot \mathsf{S}^{-1} = (0,0,1)\cdot \mathsf{S}^{-1} = (0,0,1),$$

where θ is the angle between the simulation box basis vector along the x direction and the extension direction for PEF (see Fig. 1). Only certain values of θ give reproducible lattices and we choose, for our simulations, the value of $\theta \simeq 31.7°$, already used in the literature.

The lattice generated by the vectors $\mathbf{l}_i'(0)$ in Eq. (9) is reproduced after a period of time τ_p, that is, when the system has experienced a total "Hencky" strain of $\epsilon_p = \dot{\epsilon}\tau_p = \ln(\lambda)$, where λ is the eigenvalue of the map $\nabla \mathbf{u}_{\text{elongation}}$.[9] The reproducibility time τ_p is the same for both PEF and PMF. As can be seen in Eq. (6), the shear field changes the PEF basis vectors (i.e., the tensor S^{-1}), but the evolution of the lattice is due to the PEF velocity gradient alone (i.e., the tensor D).

We now need to verify the compatibility of the lattice with our flow geometry. Kraynik and Reinelt[5] demonstrated that reproducibility guarantees compatibility, i.e., the distance $D(t)$ among the lattice points never falls below a minimum and finite value D_m, such that the lattice points do not overlap. However, we need to ensure that D_m is large enough for our purposes, i.e., is not less than the interatomic potential diameter. We are interested in the evolution of the lattice only in the xy plane; therefore, we set one corner of the cell box as the origin and express $D(t)$ in turn as the modulus of the three vectors $\mathbf{r}_i(t)$, $i=1,2,3$, representing the other three vertices of the cell box in the xy plane (see Fig. 2).

We start from the equation for the streamlines for the mixed flow, both in parametric form

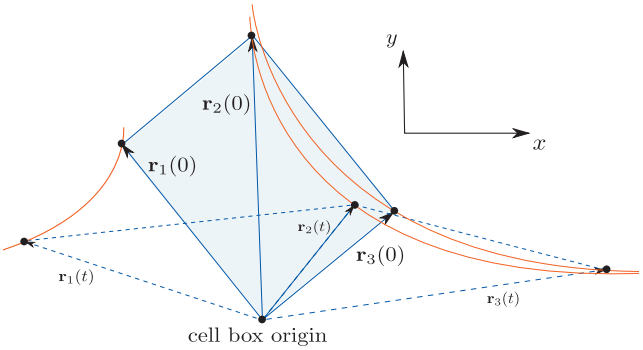

FIG. 2. Schematic representation of the vectors $\mathbf{r}_i(t)$ identifying the three vertices of the simulation box and used to verify the compatibility condition.

$$x(t) = \frac{\dot{\gamma}}{\dot{\epsilon}}y(0)\sinh(\dot{\epsilon}t) + x(0)\exp(\dot{\epsilon}t),$$

$$y(t) = y(0)\exp(-\dot{\epsilon}t), \tag{10}$$

and in nonparametric form

$$\dot{\gamma}y^2 + 2\dot{\epsilon}xy = c, \tag{11}$$

where c is a numeric constant and $x(t)$, $y(t)$ are in turn the coordinates of the three corners of the cell. Using the above expressions and solving the equation

$$\frac{d}{dt}(\mathbf{r}(t)\cdot\mathbf{r}(t)) = 2(x\dot{x} + y\dot{y}) = 0, \tag{12}$$

we calculate the time t_m at which the distance $\mathbf{r}(t)$ is a minimum, substitute it into $y(t)$ and $x(t)$, and find the distance D_m

$$t_m = \frac{1}{4\dot{\epsilon}}\ln\left(\frac{\dot{\gamma}^2y_0^2 + 4\dot{\epsilon}^2y_0^2}{(\dot{\gamma}y_0 + 2\dot{\epsilon}x_0)^2}\right), \tag{13}$$

$$y(t_m) = y_0\exp(-\dot{\epsilon}t_m), \tag{14}$$

$$D_m = \sqrt{x(t_m)^2 + y(t_m)^2} = \sqrt{\left(\frac{c - \dot{\gamma}y(t_m)^2}{2\dot{\epsilon}y(t_m)}\right)^2 + y(t_m)^2}, \tag{15}$$

where $x_0 = x(0)$ and $y_0 = y(0)$. The results show compatibility for all the cases we evaluated.

A. Noncanonical mixed flow

For canonical mixed flow, the expanding and contracting axes are determined by the directions of the velocity gradient's eigenvectors and the field strength by their modulus. For the velocity gradient in Eq. (7), we have the following eigenvalues:

$$\lambda = \pm\dot{\epsilon}. \tag{16}$$

A possible choice of eigenvectors is

$$\mathbf{u}_1 = (1,0,0), \quad \mathbf{u}_2 = \left(-1, \frac{2\dot{\epsilon}}{\dot{\gamma}}, 0\right). \tag{17}$$

The angle between them is therefore

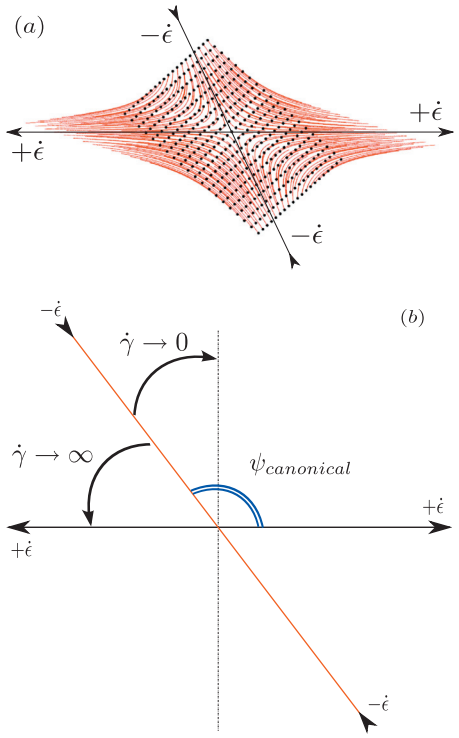

FIG. 3. (a) Initial configuration of a lattice (black dots) undergoing planar mixed flow and corresponding streamlines (red lines). The contracting and expanding axes are nonorthogonal. (b) Schematic representation of how the angle $\psi^{\text{canonical}}$ varies for the different values of shear field keeping the elongational field constant.

$$\psi_{\text{canonical}} = \cos^{-1}\left(-\frac{\dot{\gamma}}{\sqrt{\dot{\gamma}^2 + 4\dot{\epsilon}^2}}\right). \tag{18}$$

From Eqs. (8) and (18) and Fig. 3, we can see that changes to $\dot{\epsilon}$ and $\dot{\gamma}$ result in a change of the angle between the axes of expansion and contraction; however, the field along these axes assumes always the values $+\dot{\epsilon}$ and $-\dot{\epsilon}$, respectively.

As expressed in Fig. 3, if $\dot{\gamma}=0$, then $\psi_{\text{canonical}} = \pi/2 \pm n\pi$, while if $\dot{\gamma}\to\infty$, then $\psi_{\text{canonical}} = \pm n\pi$ with n an integer. This means that for the canonical mixed flow, the contraction axis always lies on a slope $y=-ax$ with $a \in \Re^+$.

We now consider a general (noncanonical) matrix $\nabla \mathbf{u}^{nc}$, where extension and contraction are along the x and y axes, respectively, but with a shear gradient oriented along an arbitrary direction

$$\nabla \mathbf{u}^{nc} = \begin{pmatrix} g\cos(\phi)\sin(\phi) + e & -g\sin(\phi)^2 & 0 \\ g\cos(\phi)^2 & -g\cos(\phi)\sin(\phi) - e & 0 \\ 0 & 0 & 0 \end{pmatrix}, \tag{19}$$

where ϕ is the angle between the contracting (y in this case) axis and the velocity gradient [negative toward the first Cartesian quadrant and positive toward the second, (see Fig. 4)]. g and e are the shear gradient and the elongational field strengths, respectively (we use different symbols to avoid confusion between the two representations).

We now show that when the noncanonical strain-rate tensor in Eq. (19) is able to generate a mixed flow, it can be expressed in a canonical form in a rotated frame. To our knowledge, this is the first time that this equivalence is shown and it means that the canonical form is able to parameterize any planar mixed flow. The expansion and contraction directions are given by the eigenvectors of the $\nabla \mathbf{u}^{nc}$ matrix; if for a given choice of $[g, e, \phi]$, we are able to find a pair $[\dot{\gamma}, \dot{\epsilon}]$, such that the angles between the eigenvectors in both canonical and noncanonical forms are the same, the two representations will be equivalent up to a rotation. For the noncanonical system we have the eigenvalues

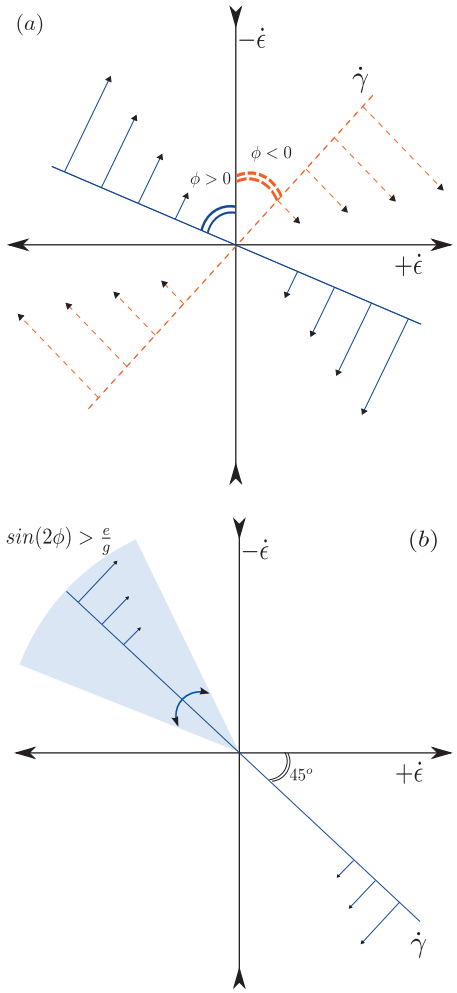

FIG. 4. (a) Schematic representation of the noncanonical flow with the strain-rate gradient tensor of Eq. (7) when varying the parameter ϕ. (b) The gray cone represents the range of shear gradient axis orientations for which the noncanonical flow of Eq. (19) degenerates into an elliptical flow.

$$\lambda = \pm\sqrt{e^2 - 2eg\sin(\phi)\cos(\phi)}, \tag{20}$$

and the following eigenvectors:

$$w_1 = \left(1, \frac{g\sin(\phi)\cos(\phi) - e + \sqrt{2eg\sin(\phi)\cos(\phi) + e^2}}{g\cos(\phi)^2}, 0\right), \tag{21}$$

$$w_2 = \left(-1, \frac{g\sin(\phi)\cos(\phi) - e - \sqrt{2eg\sin(\phi)\cos(\phi) + e^2}}{g\cos(\phi)^2}, 0\right). \tag{22}$$

Therefore the angle between them is

$$\psi_{\text{noncanonical}} = \cos^{-1}\left(-\frac{g}{\sqrt{4e^2 - 8ge\cos(\phi)\sin(\phi) + g^2}}\right). \tag{23}$$

For $\phi=0$, we fall into the canonical case. For any given set $[g,e,\phi]$, it is always possible to find a pair $[\dot{\gamma},\dot{\epsilon}]$ such that $\psi_{\text{noncanonical}}=\psi_{\text{canonical}}$, if the noncanonical eigenvalues are real, i.e.,

$$\sin(2\phi) < \frac{e}{g}. \tag{24}$$

If the eigenvalues are 0, the flow reduces to pure shear flow, while if they are imaginary, the flow becomes elliptical. The condition given by Eq. (24), visualized in Fig. 4(b), is equivalent (for any chosen values of g and e) to drawing a cone around the slope $y=-x$; this is easy to see plotting $\sin(2\phi)$ against ϕ. If the shear gradient falls inside the cone, the flow becomes elliptical. We note that there is one specific case in which the flow is a pure rotation. This happens when $\phi=45°$ and $g=2e$, that is, when the matrix $\nabla \mathbf{u}^{nc}$ is antisymmetric. Any shear flow can, in fact, be decomposed as the sum of an elongational flow plus a pure rotation. Therefore, if the shear flow component of the noncanonical mixed flow can be separated into a rotational and an elongational part, and the two elongational fields so obtained cancel each other out, what remains is just pure rotational flow.

III. ALGORITHM

Methods that perform an irreversible squeezing of the simulation cell require a careful choice of $\dot{\epsilon}$ to ensure the achievement of a steady state before the box dimension in the contracting direction reaches $2r_c$, where r_c is the cutoff distance for the potential energy function. Our algorithm does not suffer from such a drawback. We cannot, however, arbitrarily choose the simulation box dimensions. The map S^{-1} in Eq. (9) is not volume preserving but has determinant $\det(\mathsf{S}^{-1})=-2\dot{\epsilon}/\dot{\gamma}$. This map, as already pointed out, changes PEF basis vectors, making them reproducible under PMF, but while the basis vectors that generate the PEF box are equal in modulus and orthogonal, the basis vectors that generates the PMF box depend (in both modulus and direction) on the ratio between elongational and shear fields

$$\begin{aligned}
|\mathbf{l}_1'(0)| &= \sqrt{1 + \frac{\dot{\gamma}^2}{4\dot{\epsilon}^2}\sin^2\theta - \frac{\dot{\gamma}}{\dot{\epsilon}}\cos\theta\sin\theta}, \\
|\mathbf{l}_2'(0)| &= \sqrt{1 + \frac{\dot{\gamma}^2}{4\dot{\epsilon}^2}\cos^2\theta + \frac{\dot{\gamma}}{\dot{\epsilon}}\cos\theta\sin\theta}, \\
\mathbf{l}_1'(0)\cdot\mathbf{l}_2'(0) &= -\frac{\dot{\gamma}}{2\dot{\epsilon}}\cos 2\theta + \frac{\dot{\gamma}^2}{4\dot{\epsilon}^2}\sin\theta\cos\theta.
\end{aligned} \tag{25}$$

This must be taken into account when setting up the system at the beginning of a simulation. We want to stress however, that the volume of the cell box does not change with time during a specific simulation (we are in fact considering only isochoric flows). The orientations of the basis vectors are field dependent and will not in general be orthogonal. It may be convenient however, to start a simulation from a rectangular parallelepiped to be able to arrange particles on usual lattices. To recover a rectangular parallelepiped, we utilize the fact that the Hencky strain does not depend on the choice of the origin along the time axis. This means that $\mathbf{L}_i'(t^*+\tau_p)=\mathbf{L}_i'(t^*)$ for arbitrary t^*; therefore, if a time $t_\perp$ exists at which the basis vectors for the mixed flow in Eq. (25) are orthogonal, we can set $t^*=t_\perp$ as the new time origin. To obtain $t_\perp$, we impose the basis orthogonality condition, $\mathbf{l}_1'(t^*)\cdot\mathbf{l}_2'(t^*)=0$ and solve for t^*.

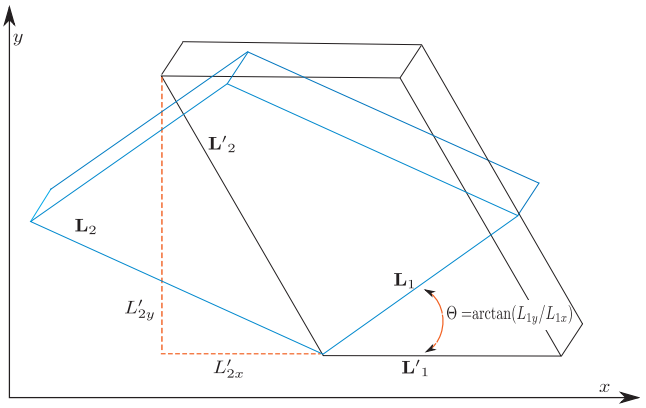

FIG. 5. Diagram outlining the PBCs and minimum image distance implementation. For each time step, the simulation box is rotated by an angle $\Theta(t)$ such that one side of the box is parallel to the x laboratory axis.

The remainder of the implementation of the PBCs follows the same procedure outlined by Todd and Daivis.[21] For each time step, the simulation cell is rotated so as to align the cell box with the laboratory x axis, making the PBC and the minimum image distance calculation much easier and improving the computational efficiency. This procedure is applied only to perform the PBCs and does not affect the particle dynamics. Once in the rotated frame, we compute the displacement of the boundaries applying Eq. (10) for the streamlines to the rotated primitive lattice vectors

$$\mathrm{L}_{kx}'(t) = \frac{\dot{\gamma}}{\dot{\epsilon}}\mathrm{L}_{ky}'(0)\sinh(\dot{\epsilon}t) + \mathrm{L}_{kx}'(t)\exp(\dot{\epsilon}t), \tag{26}$$

$$\mathrm{L}_{ky}'(t) = \mathrm{L}_{ky}'(0)\exp(-\dot{\epsilon}t), \tag{27}$$

$$\mathrm{L}_{kz}'(t) = \mathrm{L}_{kz}'(0), \tag{28}$$

where the index $k=1,2,3$ defines the lattice vectors and the primed variables refer to the rotated vectors. The angle by which the simulation box must be rotated evolves as $\Theta(t)=\arctan(\mathrm{L}_{1y}'(t)/\mathrm{L}_{1x}'(t))$ (see Fig. 5).

In order to implement our mixed flow algorithm, we use the corresponding SLLOD equations of motion for the particle dynamics,[22]

TABLE I. Elongational viscosity and shear viscosity results for an atomic fluid undergoing mixed flow with different combinations of field strengths. The fluid is thermostatted at a reduced temperature of $T=1.0$ and the density is set at $\rho=0.8442$. The errors, in brackets, are twice the standard error of the mean of five independent runs. We also report the viscosities obtained by Baranyai and Cummings (Ref. 11), where a comparison is possible.

				Baranyai and Cummings viscosities	
PEF ($\dot{\epsilon}$)	PCF ($\dot{\gamma}$)	η (PEF)	η (PCF)	η (PEF)	η (PCF)
0.1	0.1	2.196 (0.006)	2.155 (0.009)		
0.2	0.1	2.056 (0.001)	2.033 (0.006)		
0.3	0.1	1.954 (0.001)	1.93 (0.01)		
0.4	0.1	1.875 (0.001)	1.87 (0.02)		
0.5	0.1	1.823 (0.000)	1.817 (0.009)		
0.1	0.2	2.171 (0.001)	2.116 (0.003)		
0.2	0.2	2.042 (0.001)	2.007 (0.003)		
0.3	0.2	1.943 (0.001)	1.912 (0.005)		
0.4	0.2	1.873 (0.000)	1.848 (0.005)		
0.5	0.2	1.824 (0.001)	1.786 (0.005)		
0.1	0.3	2.139 (0.002)	2.065 (0.002)		
0.2	0.3	2.021 (0.002)	1.974 (0.002)		
0.3	0.3	1.933 (0.001)	1.900 (0.002)		
0.4	0.3	1.869 (0.001)	1.832 (0.004)		
0.5	0.3	1.820 (0.001)	1.773 (0.002)		
0.1	0.4	2.103 (0.003)	2.016 (0.001)		
0.2	0.4	1.996 (0.002)	1.946 (0.002)		
0.3	0.4	1.919 (0.002)	1.877 (0.002)		
0.4	0.4	1.860 (0.001)	1.821 (0.002)		
0.5	0.4	1.813 (0.001)	1.770 (0.003)		
0.1	0.5	2.068 (0.001)	1.972 (0.001)	2.12 (0.04)	1.96 (0.04)
0.2	0.5	1.970 (0.001)	1.918 (0.001)	1.97 (0.04)	1.95 (0.04)
0.3	0.5	1.901 (0.001)	1.857 (0.001)	1.91 (0.04)	1.87 (0.04)
0.4	0.5	1.846 (0.001)	1.808 (0.001)		
0.5	0.5	1.804 (0.000)	1.759 (0.001)	1.80 (0.04)	1.75 (0.04)
1.0	0.5	1.804 (0.001)	1.760 (0.002)		
0.5	1.0	1.756 (0.001)	1.692 (0.001)	1.77 (0.04)	1.70 (0.04)
1.5	1.0	1.682 (0.000)	1.591 (0.002)		
1.0	1.5	1.694 (0.001)	1.563 (0.000)		

$$\dot{\mathbf{r}}_i = \frac{\mathbf{p}_i}{m_i} + \mathbf{r}_i \cdot \nabla \mathbf{u} = \frac{\mathbf{p}_i}{m_i} + \dot{\epsilon}(x_i\hat{\mathbf{x}} - y_i\hat{\mathbf{y}}) + \dot{\gamma} y_i \hat{\mathbf{x}},$$
$$\dot{\mathbf{p}}_i = \mathbf{F}_i - \mathbf{p}_i \cdot \nabla \mathbf{u} = \mathbf{F}_i - \dot{\epsilon}(p_{xi}\hat{\mathbf{x}} - p_{yi}\hat{\mathbf{y}}) - \dot{\gamma} p_{yi}\hat{\mathbf{x}}, \tag{29}$$

coupled with a Nosé–Hoover thermostat.[23] The SLLOD equations of motion have been demonstrated to be the appropriate equations of motion for any homogeneous flow.[24,25] Other sets of equations have been proposed at different times,[26–29] but they have all been found to be deficient in some aspects.[22,25]

IV. RESULTS

To test the validity of our algorithm, we compare our viscosity data with those found in Baranyai and Cummings.[11] We simulate an atomic system interacting by the Weeks–Chandler–Anderson[30] (WCA) potential at a temperature $T=0.722$ and density $\rho=0.8442$. We use a time step of $\Delta t=0.001$. To reach the steady state, the system is equilibrated for $t=1000$ time units and a further $t=3000$ time units are used for data collection. The viscosity values and standard errors plotted in the table correspond to an averaging over five independent runs. All the physical quantities are expressed in reduced units where the unit of mass is the particle mass m, the energy unit and the length unit are the WCA parameters ϵ and σ, which are all set to unity.

From the relation between the heat production rate per unit volume and the second scalar invariant of the strain-rate tensor $II=\dot{\boldsymbol{\gamma}}:\dot{\boldsymbol{\gamma}}$, Hounkonnou *et al.*[31] derived a general expression for the viscosity of an isotropic fluid undergoing isochoric flow

$$\eta = (\boldsymbol{\sigma}:\dot{\boldsymbol{\gamma}})/(\dot{\boldsymbol{\gamma}}:\dot{\boldsymbol{\gamma}}), \tag{30}$$

where $\boldsymbol{\sigma}$ is the stress tensor and $\dot{\boldsymbol{\gamma}}$ is the strain-rate tensor. It is then possible to obtain a viscosity for the mixed flow which can also be expressed in terms of the PCF and PEF viscosities ($II=2\dot{\gamma}^2$ for PCF and $II=8\dot{\epsilon}^2$ for PEF)

$$\eta_{\text{mixed}} = \frac{-2\dot{\epsilon}P_{xx} + 2\dot{\epsilon}P_{yy} - 2\dot{\gamma}P_{xy}}{8\dot{\epsilon}^2 + 2\dot{\gamma}^2} = \frac{(8\dot{\epsilon}^2\eta(\text{PEF}) + 2\dot{\gamma}^2\eta(\text{PCF}))}{8\dot{\epsilon}^2 + 2\dot{\gamma}^2}. \tag{31}$$

We note that the formula in Eq. (31), reported in Ref. 11, contains some typographical errors.

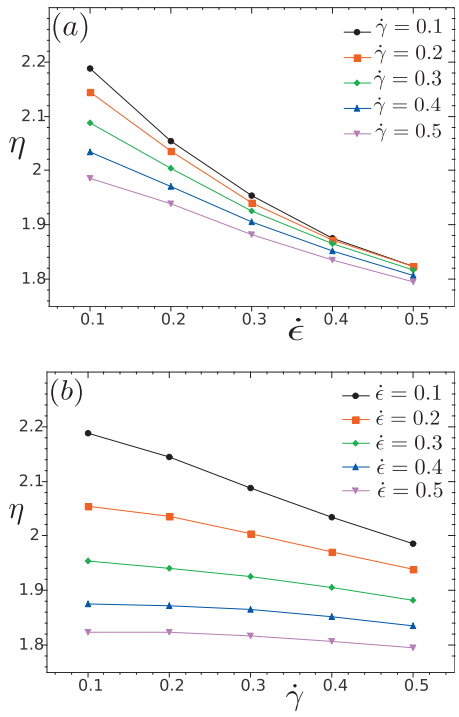

FIG. 6. Plot of the viscosity defined in Eq. (31) for an atomic fluid undergoing mixed flow with different combinations of field strengths. The fluid is thermostatted at a reduced temperature of $T=1.0$ and the density is set at $\rho=0.8442$. The error bars are not reported because they are smaller than the symbols. (a) Viscosity for the different values of elongational field (on the x axis) at fixed shear fields. (b) Viscosity for the different values of shear field (on the x axis) at fixed elongational fields.

In Table I we report only the PEF and PCF viscosities defined as

$$\eta_{\mathrm{PEF}} = \frac{P_{yy} - P_{xx}}{4\dot{\epsilon}}, \quad \eta_{\mathrm{PCF}} = -\frac{P_{xy}}{\dot{\gamma}} \tag{32}$$

and we report the general viscosity η_{mixed} in Fig. 6 to easily compare the results. Our viscosities agree very well with those computed by Baranyai and Cummings (see Table I). Finally we note from Fig. 6 that the elongational field affects the viscosity more than the shear field. The viscosity thinning is more pronounced when the elongational field increases and the shear field is kept constant rather than the other way around.

V. CONCLUSION

In this work we have derived and implemented an algorithm for indefinite NEMD simulation of fluids under mixed flow. To accomplish this, we used results from the theory of lattices. Similar to PEF simulation techniques,[21] the cell box deforms according to the flow streamlines and is remapped to its original shape after a fixed amount of time without discontinuities in physical properties. Statistics are therefore improved and a broad range of fluids, such as dense alkanes or polymer melts, can be investigated. Our viscosity results are validated with previous data[11] obtained with a finite-time algorithm. To conclude, we have also shown (for the first time, to our knowledge) that a mixed flow in which the shear and elongation axes are not orthogonal is equivalent to one in which they are orthogonal, for an appropriate choice of field parameters.

[1] N. J. Woo and E. S. G. Shaqfeh, J. Chem. Phys. **119**, 2908 (2003).
[2] A. W. Lees and S. F. Edwards, J. Phys. C: Solid State Phys. **5**, 1921 (1972).
[3] P. M. Adler and H. Brenner, Int. J. Multiphase Flow **11**, 361 (1985).
[4] R. Bhupathiraju, P. T. Cummings, and H. D. Cochran, Mol. Phys. **88**, 1665 (1996).
[5] A. M. Kraynik and D. A. Reinelt, Int. J. Multiphase Flow **18**, 1045 (1992).
[6] P. M. Adler, M. Zuzovsky, and H. Brenner, Int. J. Multiphase Flow **11**, 387 (1985).
[7] B. D. Todd and P. J. Daivis, Phys. Rev. Lett. **81**, 1118 (1998).
[8] A. Baranyai and P. T. Cummings, J. Chem. Phys. **110**, 42 (1999).
[9] T. A. Hunt and B. D. Todd, Mol. Phys. **101**, 3445 (2003).
[10] M. L. Matin, P. J. Daivis, and B. D. Todd, Comput. Phys. Commun. **151**, 35 (2003).
[11] A. Baranyai and P. T. Cummings, J. Chem. Phys. **103**, 10217 (1995).
[12] A. Dua and B. J. Cherayil, J. Chem. Phys. **119**, 5696 (2003).
[13] B. D. Hoffman and E. Shaqfeh, J. Rheol. **51**, 947 (2007).
[14] B. D. Todd, Phys. Rev. E **58**, 4587 (1998).
[15] P. J. Daivis and B. D. Todd, Int. J. Thermophys. **19**, 1063 (1998).
[16] B. D. Todd and P. J. Daivis, J. Chem. Phys. **107**, 1617 (1997).
[17] P. Ilg, H. C. Öttinger, and M. Kröger, Phys. Rev. E **79**, 011802 (2009).
[18] T. A. Hunt, Ph.D. thesis, Swinburne University of Technology, 2008.
[19] G. G. Fuller and L. G. Leal, J. Polym. Sci., Polym. Phys. Ed. **19**, 557 (1981).
[20] R. G. Larson, *The Structure and Rheology of Complex Fluids* (Oxford University Press, New York, 1999).
[21] B. D. Todd and P. J. Daivis, Comput. Phys. Commun. **117**, 191 (1999).
[22] B. D. Todd and P. J. Daivis, Mol. Simul. **33**, 189 (2007).
[23] W. G. Hoover, Phys. Rev. A **31**, 1695 (1985).
[24] D. J. Evans and G. P. Morriss, Phys. Rev. A **30**, 1528 (1984).
[25] P. J. Daivis and B. D. Todd, J. Chem. Phys. **124**, 194103 (2006).
[26] C. Baig, B. J. Edwards, D. J. Keffer, and H. D. Cochran, J. Chem. Phys. **122**, 184906 (2005).
[27] C. Baig, B. J. Edwards, D. J. Keffer, and H. D. Cochran, J. Chem. Phys. **122**, 114103 (2005).
[28] B. J. Edwards and M. Dressler, J. Non-Newtonian Fluid Mech. **96**, 163 (2001).
[29] M. E. Tuckerman, C. J. Mundy, S. Balasubramanian, and M. L. Klein, J. Chem. Phys. **106**, 5615 (1997).
[30] J. D. Weeks, D. Chandler, and H. C. Andersen, J. Chem. Phys. **54**, 5237 (1971).
[31] M. N. Hounkonnou, C. Pierleoni, and J. P. Ryckaert, J. Chem. Phys. **97**, 9335 (1992).